Growth front roughening of room-temperature deposited copper nanocluster films

Palasantzas, G.; Koch, S. A.; de Hosson, J. Th. M.

Published in:
Applied Physics Letters

DOI:
10.1063/1.1497200

Growth front roughening of room-temperature deposited copper nanocluster films

G. Palasantzas, S. A. Koch, and J. Th. M. De Hosson[a)]
Department of Applied Physics, Materials Science Centre and the Netherlands Institute for Metals Research, University of Groningen, Nijenborgh 4, 9747 AG Groningen, The Netherlands

(Received 18 February 2002; accepted for publication 3 June 2002)

Growth front aspects of copper nanocluster films deposited with low energy onto silicon substrates at room temperature are investigated by atomic force microscopy. Analyses of the height-difference correlation function yield a roughness exponent H of 0.45 ± 0.05. The root-mean-sqaure roughness amplitude w evolves with deposition time as a power law, $w\propto t^{\beta}$ ($\beta=0.62\pm0.07$), leading also to a power-law increase of the local surface slope ρ, $\rho\propto t^{c}$ ($c=0.73\pm0.09$). These scaling exponents, in combination with an asymmetrical height distribution, point at a complex nonlinear roughening mechanism dominated by the formation of voids resulting in a highly porous film. © *2002 American Institute of Physics.* [DOI: 10.1063/1.1497200]

The growth of thin films by direct deposition of nanoclusters has attracted considerable interest, both from a fundamental and a technological point of view.[1–4] The advantage of the method is that well-adhered metallic films can be produced on a wide variety of substrates. Film density and surface area to volume ratio may be controlled by an appropriate selection of the kinetic energy of impact and the number of atoms per cluster. This methodology provides, therefore, the possibility of thin film applications.

The influence of kinetic energy of impinging clusters has been investigated by Haberland *et al.*[1] using molecular dynamics for Mo cluster deposition on Mo(001) substrates. The effect ranges from light cluster flattening upon impact (at 0.1 eV/atom) to complete fragmentation at higher energies (10 eV/atom). In the latter case, the cluster temperature increases strongly in a self-annealing process, leading to the formation of a dense film. For low impact energy, a rather porous film is obtained. Fuchs *et al.*[2] have shown that the deposition rate and the mean size of Sb clusters control aspects of crystallinity and coverage rate of Sb films on amorphous carbon substrates. Zimmermann *et al.*[3] observed that Co nanoparticles in the 10 nm size range submerge into clean Cu(100) and Ag(100) substrates when deposited at 600 K, while at room temperature, submersion did not occur.

So far, few studies have explicitly considered scaling aspects of the surface morphology for nanocluster films, and their relation to microscopic film growth mechanisms. Moseler *et al.*[5] reported an Edwards–Wilkinson type of growth for highly energetic (~5 eV/atom) Cu clusters onto Si. Growth studies for low-energy (<0.5 eV/atom) deposited C clusters on Si and Cu by Buzio *et al.*,[6] using atomic force microscopy (AFM), yielded roughness and growth exponents, respectively, $H=0.64-0.68$ and $\beta=0.42-0.50$ (largely independent on the average cluster size, although the presence of large particles within the cluster beam induced significant morphology fluctuations).[6] For C particles, the covalent bonding prohibits cluster coalescence. In this work, we perform analysis of low-energy Cu nanocluster deposition with a narrow size distribution while the metallic nature of Cu makes cluster coalescence more likely to occur.

Deposition was performed using a nanocluster source from Oxford Applied Research based on the gas aggregation technique (which offers a relatively narrow cluster size distribution) developed by Haberland.[1] Atoms are sputtered in a magnetron device, after which they combine in a flow of rare gas (Ar) to form clusters. The base chamber pressure was $\sim10^{-8}$ mbar, while during sputtering with Ar gas, it was $\sim10^{-3}$ mbar. The sputtering magnetron power was 60 W (300 V and plasma current 0.2 A). The deposition rate was ~4.5 nm/min, as determined afterward by Auger depth profile analysis. A deposition time of 2 min corresponds to the percolation threshold (sufficient to obtain a closed film). Substrates about 100 mm^2 in size were cut from Si(100) wafers and were treated with a 40% HF solution to remove the native oxide prior to deposition.

The film surface morphology was characterized in air (relative humidity $\sim45\%$) using a Digital Instruments Dimension 3100 AFM, which was operated in tapping mode[7] to minimize damage of the film surface. The cantilever oscillation amplitude was maintained by a feedback loop with a setpoint value ~1.0 V. Clusters could be attached to the tip resulting in distorted images due to multiple-tip effects. Image reproducibility was verified by repeated scans over the same area to exclude any tip effects. The AFM tip and cantilever are an integrated assembly of single crystal silicon (produced by etching). The tip radius is $\leqslant10$ nm with a side angle $\leqslant10°$. Transmission electron microscopy (TEM) on simultaneously exposed Si_3N_4 membrane substrates revealed a supported cluster size of the order of 10 nm, i.e., comparable to the AFM tip radius. Although isolated clusters can be resolved with AFM [Fig. 1(a),] tip convolution has significant influence on the observed lateral size of such clusters.[8]

Upon impingement of Cu clusters on the Si substrate, cluster coalescence and partial submersion into the substrate surface occur [Fig. 1(b): deflection image which shows the change of the cantilever deflection amplitude recorded simultaneously with the height data]. We can estimate the time

a)Author to whom correspondence should be addressed; electronic mail: hossonj@phys.rug.nl

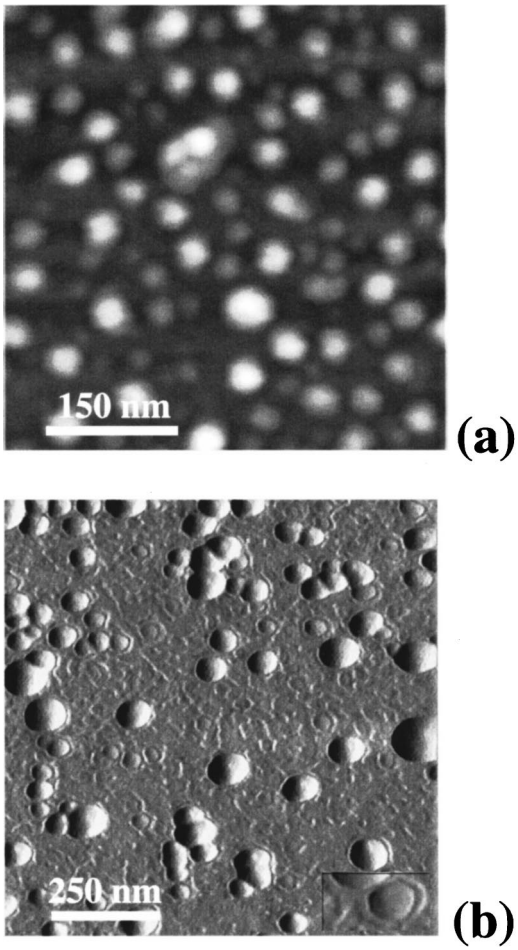

FIG. 1. (a) AFM topography image (500 nm scan size) of an open film etched with HF to remove any Si oxide around the nanoclusters. (b) AFM deflection image (scan size 1 μm) of an open Cu nanocluster film showing partial submersion into the Si surface. The inset shows a magnified image of a submerged cluster.

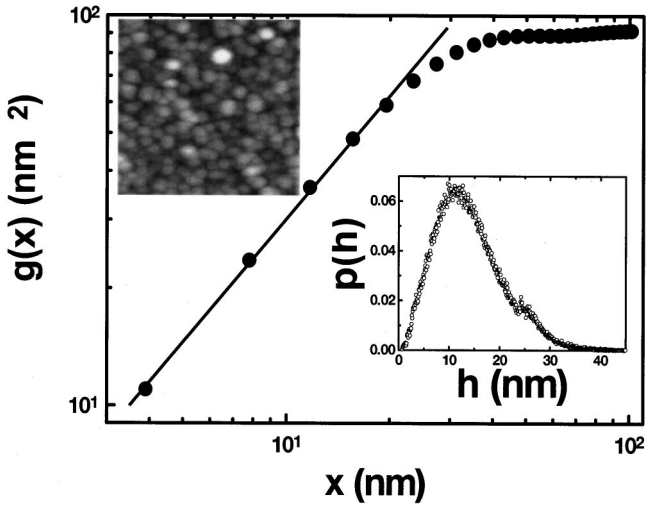

FIG. 2. Height-difference correlation function vs lateral scale x. The actual scan size in the measurement of $g(x)$ is 2 μm. The linear fit yields the roughness exponent $H=0.49\pm0.03$. The saturation regime yields $w=6.7$ nm, and for the correlation length, we obtain $\xi=31$ nm which is comparable with the average particle size in the AFM image (upper inset; scan size 500 nm). The lower inset shows the asymmetrical height distribution.

"τ" for two spheres of radius R_{Cu} to coalesce and form one sphere by grain boundary diffusion as $\tau=[A(k_BT)/V_m\gamma_{\mathrm{Cu}}(\delta D)]R_{\mathrm{Cu}}^4(X/R_{\mathrm{Cu}})^6$ (Refs. 3 and 9–11) with $A=0.0125$[10,12] $V_m\approx9.1\times10^{-30}$ m^3 represents the volume of one Cu atom, $\gamma_{\mathrm{Cu}}=1.75$ J/m^2 is the surface energy of Cu [for Cu(001)],[3] and $(\delta D)=2.\times10^{-14}\exp(-105\ \mathrm{kJmol^{-1}/RT})$ m^3/s is the grain-boundary diffusivity of Cu with δ, the interface width along which diffusion occurs.[13,14] The factor (X/R) is the ratio between the neck size and the cluster radius. In the initial stage with X/R small, say 0.1, we estimate $\tau\cong0.25$ s at room temperature for $R_{\mathrm{Cu}}=5$ nm. Therefore, such a process is reasonably fast to occur during cluster deposition. Furthermore, the presence of a rim around the clusters indicates a partial submersion into the substrate, whereby clusters are partly covered by substrate material. This can be explained by the higher surface energy of Cu than that of $Si(\gamma_{\mathrm{Si}}=1.4\ \mathrm{J/m^2})$.[15] Submergence is driven by large capillary forces on the clusters, and it occurs if the cluster has sufficient kinetic energy and significantly higher surface energy than the substrate.[3]

For each film, the height-difference correlation function $g(x)=\langle[h(x)-h(0)]^2\rangle$ in the fast scan direction was computed, with $h(x)$ the surface height at lateral position $x(\langle h(x)\rangle=0)$. The results were averaged over five AFM topography images (with 512 points/line scan) acquired at different locations on the film surface (Fig. 2). For a self-affine rough morphology, we have $g(x)=\rho^2x^{2H}$ for $x\ll\xi$ and $g(x)=2w^2$ for $x\gg\xi$ (with ξ the lateral correlation length and $\rho\propto w/\xi^H$ the average local surface slope).[16–18] The root-mean-square (rms) roughness amplitude w can be obtained from the saturated regime of $g(x)$, while a double log plot at shorter length scales yields the roughness exponent H. As H decreases, the surface becomes more irregular (jagged) at short length scales $(x\ll\xi)$.[16–18] Finally, the intersection of power-law and saturation lines gives the correlation length $\xi=(2w^2/\rho^2)^{1/2H}$.

The height distribution $P(h)$ shows deviations from pure Gaussian behavior. To quantify this point further, we calculated the skewness $S=\int h^3[P(h)/\int P(h)dh]dh/w^3$, which is a measure of the distribution symmetry around a reference surface level. For a Gaussian distribution $S=0$, while in the present case we obtained for all film thickness $S>0$, indicating that the $h\leftrightarrow-h$ symmetry is broken. This can be attributed to a nonlinearity associated with the dependence of growth on the local surface inclination.[18]

Calculated values of w, H, and ρ for each deposition time t are shown in Fig. 3. The growth of the rms amplitude w is quantified by the growth exponent $\beta=0.62\pm0.07$ as $w\propto t^{\beta}$.[16–18] The roughness exponent H was found to be $H=0.45\pm0.05$. The average local surface slope $\rho(\propto w/\xi^H)$ increases with deposition time as a power-law $\rho\propto t^c$ with $c=0.73\pm0.09$, which is even more evidence of surface roughening. Although the rms amplitude w increases with growth time, the correlation length ξ saturates to a value ~34–40 nm for later stages of growth indicating the development of limited lateral correlations.

Due to the influence of the finite AFM tip curvature, the actual roughness exponents H might be slightly smaller than the obtained values of $H=0.45\pm0.05$,[19] but they appear to be close to that predicted by the Kardar-Parisi-Zhang (KPZ) model, $H\approx0.4$.[20,21] In this model, the dominant relaxation mechanisms are desorption or the formation of pores.[17,18] In our case, porosity is formed as a result of soft landing of the

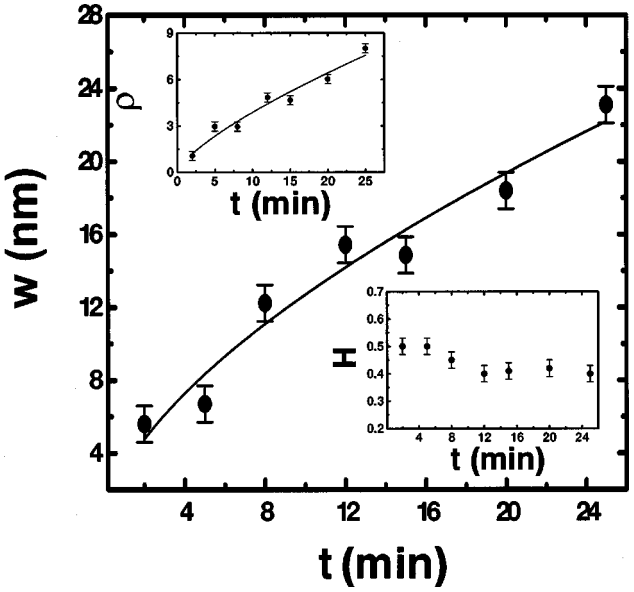

FIG. 3. The rms roughness amplitude w grows as a power law with deposition time t. The fit yields an exponent $\beta=0.61\pm0.07$. The upper inset shows the evolution of the local surface slope ρ which also grows as a power law with an exponent $c=0.73\pm0.09$. The lower inset shows the roughness exponents H vs growth time t that fall within the range $H=0.45\pm0.05$.

Cu clusters,[1] which have a limited mobility afterward. The low film density was also confirmed by x-ray reflectivity measurements ($\sim$50% of bulk Cu). However, the different growth exponent ($\beta\approx0.62$) than that of the KPZ scenario ($\beta_{\mathrm{KPZ}}\approx0.25$) can be attributed to local diffusion processes that eventually lead to cluster coalescence.

Surface diffusion of deposited clusters (as a whole) would result in a different roughness exponent, i.e., $H>0.6$.[22,23] Moreover, during early deposition stages (prior to film closure), the diffusion coefficient of a deposited cluster scales with the size or number of atoms n within the cluster as $D_n=D_1/n^c$ $(c>0)$.[2,24] This will lead to very small diffusion coefficients ($D_n \ll D_1$) for clusters of a size much larger than 10 nm. In fact, for $c=0.3-1.7$ (Refs. 2 and 24) and $n\approx3.6\times10^5$ (for a cluster diameter of 10 nm), we can estimate the ratio $D_n/D_1\cong0.02$ which excludes the diffusion of entire Cu clusters to play a predominant role as a surface relaxation mechanism.

In conclusion, we investigated growth front aspects of Cu nanocluster films deposited onto Si substrates at room temperature. The asymmetrical height distribution and the measured scaling exponents point at a complex nonlinear roughening mechanism, dominated by the high porosity. The film growth mode has similarities with the KPZ scenario, where a deposited cluster becomes part of the aggregate when it meets another cluster. However, it appears that deviations from a pure KPZ type of growth are caused by subsequent local cluster coalescence effects.

The authors acknowledge financial support from the Materials Science Center (MSC^+ program) and the Netherlands Institute for Metals Research. They thank T. Vystavel for TEM analysis of Cu clusters, T. Hibma for x-ray reflectivity measurements, and J. Krug for useful correspondence.

[1] H. Haberland, M. Moseler, Y. Qiang, O. Rattunde, T. Reiners, and Y. Thurner, Surf. Rev. Lett. **3**, 887 (1996).
[2] G. Fuchs, P. Melinon, F. Santos Aires, M. Treilleux, B. Cabaud, and A. Hoareau, Phys. Rev. B **44**, 3926 (1991).
[3] C. G. Zimmermann, M. Yeadon, K. Nordlund, J. M. Gibson, R. S. Averback, U. Herr, and K. Samwer, Phys. Rev. Lett. **83**, 1163 (1999).
[4] P. Jensen, Rev. Mod. Phys. **71**, 1695 (1999).
[5] M. Moseler, O. Rattunde, J. Nordiek, and H. Haberland, Phys. Rev. B **164**, 522 (2000).
[6] R. Buzio, E. Gnecco, C. Boragno, U. Valbusa, P. Piseri, E. Barborini, and P. Milani, Surf. Sci. **444**, L1 (2000).
[7] D. Sarid, Scanning *Force Microscopy with Applications to Electric, Magnetic and Atomic Forces*, revised edition (Oxford University Press, New York, 1994).
[8] G. L. Hornyak, S. Peschel, T. Sawitowski, and G. Schmid, Micron **29**, 183 (1998).
[9] M. Y. Chu, M. N. Rahaman, and L. C. de Jonghe, J. Am. Ceram. Soc. **74**, 1217 (1991)
[10] J. R. Blachere, A. Sedehi, and Z. H. Meiksin, J. Mater. Sci. **19**, 1202 (1984).
[11] R. M. German, *Sintering Theory and Practice* (Wiley, New York, 1996), p. 100.
[12] R. L. Coble, J. Appl. Phys. **34**, 1679 (1963).
[13] A. P. Sutton and R. W. Balluffi, *Interfaces in Crystalline Materials* (Oxford University Press, New York, 1995) pp. 792–793.
[14] I. Kaur, W. Gust, and L. Kozma, *Handbook of Grain and Interface Boundary Diffusion Data* (Ziegler, Stuttgart, 1989).
[15] D. J. Eaglesham, A. E. White, L. C. Feldman, N. Moriya, and D. C. Jacobson, Phys. Rev. Lett. **70**, 1643 (1993).
[16] Y. P. Zhao, G.-C. Wang, and T.-M. Lu, *Characterization of Amorphous and Crystalline Rough Surfaces-principles and Applications*, Experimental Methods in the Physical Science Vol. 37 (Academic, New York, 2000).
[17] J. Krim and G. Palasantzas, Int. J. Mod. Phys. B **9**, 599 (1995).
[18] P. Meakin, *Fractals, Scaling, and Growth Far from Equilibrium* (Cambridge University Press, Cambridge, UK, 1998).
[19] J.-J Aué and J. Th. M. De Hosson, Appl. Phys. Lett. **71**, 1347 (1997).
[20] M. Kardar, G. Parisi, and Y. C. Zhang, Phys. Rev. Lett. **56**, 889 (1986).
[21] T. Halpin-Healy, Phys. Rev. Lett. **254**, 215 (1995); M. Forest and L.-H. Tang, Phys. Rev. Lett. **64**, 1405 (1991).
[22] W. E. Wolf and J. Villain, Europhys. Lett. **13**, 389 (1990).
[23] Z.-W. Lai and S. Das Sarma, Phys. Rev. Lett. **66**, 2348 (1991).
[24] D. Kashchiev, Surf. Sci. **55**, 477 (1976); B. Lewis, *ibid.* **21**, 289 (1970).